Variational mean-field approach to the double-exchange model

J. L. Alonso,[1] L. A. Fernández,[2] F. Guinea,[3] V. Laliena,[1] and V. Martín-Mayor[4]
[1]*Departamento de Física Teórica, Facultad de Ciencias, Universidad de Zaragoza, 50009 Zaragoza, Spain*
[2]*Departamento de Física Teórica, Facultad de C. C. Físicas, Universidad Complutense de Madrid, 28040 Madrid, Spain*
[3]*Instituto de Ciencia de Materiales (CSIC), Cantoblanco, 28049 Madrid, Spain*
[4]*Dipartimento di Fisica, Università di Roma ''La Sapienza,'' Piazzale Aldo Moro 2, 00185 Roma, Italy and INFN Sezione di Roma, Italy*
(Received 31 July 2000; published 4 January 2001)

It has been recently shown that the double exchange Hamiltonian, with weak antiferromagnetic interactions, has a richer variety of first- and second-order transitions than previously anticipated, and that such transitions are consistent with the magnetic properties of manganites. Here we present a thorough discussion of the variational mean-field approach that leads to these results. We also show that the effect of the Berry phase turns out to be crucial to produce first-order paramagnetic-ferromagnetic transitions near half filling with transition temperatures compatible with the experimental situation. The computation relies on two crucial facts: the use of a mean-field *ansatz* that retains the complexity of a system of electrons with off-diagonal disorder, not fully taken into account by the mean-field techniques, and the small but significant antiferromagnetic superexchange interaction between the localized spins.

DOI: 10.1103/PhysRevB.63.054411 PACS number(s): 75.10.−b, 75.30.Et

I. INTRODUCTION

Doped manganites show many unusual features, the most striking being the colossal magnetoresistance (CMR) in the ferromagnetic (FM) phase.[1–3] In addition, the manganites have a rich phase diagram as a function of band filling, temperature, and chemical composition. The broad features of these phase diagrams can be understood in terms of the double exchange model (DEM),[4,5] although Jahn-Teller deformations[6] and orbital degeneracy may also play a role.[7] A remarkable property of these compounds is the existence of inhomogeneities in the spin and charge distributions in a large range of dopings, compositions, and temperatures.[8–10] In fact, for materials displaying the largest CMR effects, the size of the phase-separated domains is so large [$\sim 0.5\ \mu$m (Ref. 9)], that the electrostatic stability of the material should be addressed by theorists. At band fillings where CMR effects are present, $x \sim 0.2-0.5$, these compounds can be broadly classified into those with a high Curie temperature and a metallic paramagnetic (PM) phase, and those with lower Curie temperatures and an insulating magnetic phase.[11–13]

The double exchange mechanism was introduced by Zenner[4] through the following Kondo lattice type model

$$H_{\mathrm{KM}} = \sum_{i,j,\alpha} t_{ij} c^{\dagger}_{i\alpha} c_{j\alpha} + J_{\mathrm{H}} \sum_{i,\alpha,\alpha'} \boldsymbol{S}_i \cdot c^{\dagger}_{i\alpha} \boldsymbol{\sigma}_{\alpha\alpha'} c_{i\alpha'}, \qquad (1)$$

where t and J_{H} are, respectively, e_{g} electron's hopping and Hund's coupling between the e_{g} and the localized $t_{2\mathrm{g}}$ electrons responsible for the core spin $\boldsymbol{S}$.

When J_{H} is larger than the width of the conduction band, the model can be reduced to the double exchange model with weak interatomic antiferromagnetic (AFM) interactions. Early investigations[14] showed a rich phase diagram, with AFM, canted, and FM phases, depending on doping and the strength of the AFM couplings. More recent studies have shown that the competition between the double exchange and the AFM couplings leads to phase separation into AFM and FM regions, suppressing the existence of canted phases.[15–18] In addition, the double exchange mechanism alone induces a change in the order of the FM transition, which becomes of first order, and leads to phase separation, at low doping.[19] Note, however, that a systematic study of the nature of the transition at finite temperature was not addressed until recently,[20] despite its obvious relevance to the experiments. In fact, in Ref. 20 it was shown that a small AFM uniform superexchange interaction between the localized $t_{2\mathrm{g}}$ spins is crucial to understand some of the more relevant features of the phase diagram of the manganites. In particular a first-order phase transition is found between the PM and FM phases in the range $x \sim 0.2-0.5$. This transition does not involve a significant change in electronic density, so that domain formation is not suppressed by electrostatic effects. Therefore, we find a phase separation of a rather different type of the previously discussed, not driven by a charge instability, but by a *magnetic* instability. In addition to this phase transition, we recover those previously discussed.

In this work we give a detailed exposition of the variational mean-field technique[20] and emphasis is made on the importance of the Berry phase for the existence of first-order phase transitions near half filling. We have been able to achieve a more complete description of the phase diagram than in previous work, because we have taken full profit of a very particular feature of the DEM, namely, fermions are bilinearly coupled to *classical* degrees of freedom (the Mn spins). This allows us to trace out the fermions, thus obtaining a nonlocal effective Hamiltonian for the spins, that can be explicitly written down in terms of the density of states of the fermionic hopping matrix. What we propose to do is to calculate *exactly* the effective spin-Hamiltonian, for a given (disordered in general) configuration of the spins, using the so-called *moments-method*[21] complemented with a standard

truncation procedure.[22] This technique can be directly used for other models, like for instance models of classical spins and lattice vibrations coupled to fermions without direct interactions,[6] or also in contexts different from the manganites physics like the pyrochlores or double perovskytes. Once electrons are traced out, we study the spin thermodynamics using the variational version of the Weiss mean-field method.[23]

The main difference of our approach and previous work is that we use the exact spin Hamiltonian, while an approximated form was used up to now. For instance, the effective crystal approximation, which amounts to consider that electrons move on a perfect crystal, with a magnetically reduced hopping, was employed in Ref. 14 (see section VIII for a comparison with our method). A more accurate estimate of the density of states, well known from the physics of disordered systems and which becomes exact on the infinite-dimensions limit,[19] is the coherent potential approximation (CPA). Notice that for non-self-interacting electrons the dynamical mean-field approximation (DMFA)[24,25] is also equivalent to a CPA calculation on a given mean field, which is determined via self-consistency equations (both the mean-field and the CPA density of states are obtained self-consistently). Although those approaches are reasonable, and provide useful information, they are approximated in two different ways, which is undesiderable because two different effects are entangled. First, even for only-spins models of magnetism (like the Ising Model) where the exact spin Hamiltonian can be evaluated easily, the mean-field approximation neglects the spatial correlations of the statistical fluctuations of the order parameter (see, e.g., Ref. 23). But, in addition, for an electron-mediated magnetic interaction, the evaluation of the effective spin Hamiltonian is only accurate in the limit of infinite dimensions. With our approach, the correlations on the magnetic fluctuations are to be blamed for all the differences between our results and the real behavior of the model. On the other hand, in Sec. VIII we show how the failure of the effective-crystal approximation on finding the first-order phase transition at half filling is due to the inaccuracy on the calculation of the density of states. Moreover, we are able to study directly in three dimensions some rather subtle details, like the non-negligible effects of keeping the Berry phase on the DEM Hamiltonian.

The structure of the paper is as follows. In Sec. II we introduce the DEM and our notations. In Sec. III we present our mean-field approximation. The very nontrivial part of the work, the computation of the density of states, is explained in Sec. IV. It requires numerical simulations that can be performed on large lattices with a high accuracy. They are described in Sec. V. The effects of the Berry phase are analyzed in Sec. VI. Section VII is devoted to the study of the influence of the Berry phase in the phase diagram of the DEM. The comparison of the mean-field approach studied in this work with the de Gennes'[14] and with the DMFA is carried out in Sec. VIII. The conclusions are summarized in Sec. IX.

II. MODEL

We study a cubic lattice with one orbital per site. At each site there is also a classical spin. The coupling between the conduction electron and this spin is assumed to be infinite, so that the electronic state with spin antiparallel to the core spin can be neglected. Finally, we include an AFM coupling between nearest-neighbor core spins. We neglect the degeneracy of the conduction band. Thus, we cannot analyze effects related to orbital ordering, which can be important in the highly doped regime, $x>0.5$ (Refs. 7 and 26) (see, however, Ref. 27). We also neglect the coupling to the lattice. We focus on the role of the magnetic interactions only. As mentioned below, magnetic couplings suffice to describe a number of discontinuous transitions in the regime where CMR effects are observed. These transitions modify substantially the coupling between the conduction electrons and the magnetic excitations. Thus, they offer a simple explanation for the anomalous transport properties of these compounds. Couplings to additional modes, like optical or acoustical phonons, will enhance further the tendency towards first-order phase transitions. We consider that a detailed understanding of the role of the magnetic interactions is required before adding more complexity to the model. Note that there is indeed evidence that, in some compounds, the coupling to acoustical phonons[28] or to Jahn-Teller distortions[29] is large.

The Hamiltonian of the DEM is

$$\mathcal{H}=\sum_{ij}\ \mathcal{T}(\boldsymbol{S}_i,\boldsymbol{S}_j)c_i^{\dagger}c_j+\sum_{ij}\ \tilde{J}_{\mathrm{AF}}S^2\boldsymbol{S}_i\cdot\boldsymbol{S}_j, \tag{2}$$

where $S=3/2$ is the value of the spin of the core, Mn^{3+}, and $\boldsymbol{S}$ stands for a unit vector oriented parallel to the core spin, which we assume to be classical. In the following, we will use $J_{\mathrm{AF}}=\tilde{J}_{\mathrm{AF}}S^2$. Calculations show that the quantum nature of the core spins does not induce significant effects.[17] In one of the earliest studies of this model,[14] the superexchange coupling was chosen FM between spins lying on the same $z=constant$ plane, and AFM between spins located on neighboring planes. This is a reasonable starting point for the study of $La_{1-x}Ca_xMnO_3$ if $x<0.16$, where *A*-type antiferromagnetism is found. For larger doping, $0.16<x<0.5$, which is our main focus, the magnetism is uniform and there is no *a priori* reason for favoring a particular direction.

The function

$$\mathcal{T}(\boldsymbol{S}_i,\boldsymbol{S}_j)=t\left[\cos\frac{\theta_i}{2}\cos\frac{\theta_j}{2}+\sin\frac{\theta_i}{2}\sin\frac{\theta_j}{2}\,\mathrm{e}^{\mathrm{i}(\varphi_i-\varphi_j)}\right] \tag{3}$$

stands for the overlap of two spin 1/2 spinors oriented along the directions defined by $\boldsymbol{S}_i$ and $\boldsymbol{S}_j$, whose polar and azimuthal angles are denoted by θ and φ, respectively. It defines a hopping matrix $\mathcal{T}$, whose matrix elements are $\mathcal{T}_{ij}=\mathcal{T}(\boldsymbol{S}_i,\boldsymbol{S}_j)$. The hopping function can be written as

$$\mathcal{T}(\boldsymbol{S}_i,\boldsymbol{S}_j)=t\cos\frac{\vartheta_{ij}}{2}\exp(\mathrm{i}\phi_{ij}), \tag{4}$$

where ϑ_{ij} is the relative angle between $\boldsymbol{S}_i$ and $\boldsymbol{S}_j$, and ϕ_{ij} is the so-called Berry phase. It is sometimes assumed that the Berry phase can be set to zero without essential loss. It is therefore interesting to study the model that ignores the Berry phase, the hopping matrix being

$$\mathcal{T}_{ij}^{\mathrm{mod}}=|\mathcal{T}_{ij}|=\cos\frac{\vartheta_{ij}}{2}=\sqrt{\frac{1+\boldsymbol{S}_i\cdot\boldsymbol{S}_j}{2}}. \tag{5}$$

In the following sections we will analyze both models, with the Berry phase (hopping matrix $\mathcal{T}$) and without the Berry phase (hopping matrix $\mathcal{T}^{\mathrm{mod}}$).

III. MEAN-FIELD APPROXIMATION

Our approach to the problem follows the variational formulation of the mean-field approximation, described for instance in Ref. 23. We start by writing the grand canonical partition function for the DEM:

$$\mathcal{Z}_{\mathrm{GC}}=\int [dS]\mathrm{Tr}^{(\mathrm{Fock})}\exp[-(\mathcal{H}-\mu\mathcal{N})/T], \tag{6}$$

where μ is the electronic chemical potential, $\mathcal{N}=\Sigma_i c_i^\dagger c_i$ is the electron number operator, T is the temperature, and we use units in which the Boltzmann constant is one. The trace, taken over the electron Fock space, defines an effective Hamiltonian for the spins,

$$\exp[-\mathcal{H}^{\mathrm{eff}}(\boldsymbol{S})/T]=\mathrm{Tr}^{(\mathrm{Fock})}\exp[-(\mathcal{H}-\mu\mathcal{N})/T], \tag{7}$$

that can be computed in terms of the eigenvalues, E_n, of the hopping matrix, $\mathcal{T}$:

$$\mathcal{H}^{\mathrm{eff}}(\boldsymbol{S})=J_{\mathrm{AF}}\sum_{\langle ij\rangle}\boldsymbol{S}_i\cdot\boldsymbol{S}_j-T\times\sum_n\ln\{1+\exp[-(E_n(\boldsymbol{S})-\mu)/T]\}. \tag{8}$$

Introducing the density of states (DOS) of $\mathcal{T}$:

$$g(E;\boldsymbol{S})=\frac{1}{V}\sum_{n=1}^{V}\delta[E-E_n(\boldsymbol{S})], \tag{9}$$

where V is the volume of the lattice, the effective Hamiltonian can be written as

$$\mathcal{H}^{\mathrm{eff}}(\boldsymbol{S})=\sum_{\langle ij\rangle}J_{\mathrm{AF}}\boldsymbol{S}_i\cdot\boldsymbol{S}_j-TV\int dE\,g(E;\boldsymbol{S})\times\ln[1+e^{-(E-\mu)/T}]. \tag{10}$$

The grand canonical partition function becomes an integral in spin-configuration space:

$$\mathcal{Z}_{\mathrm{GC}}=\int [dS]\exp[-\mathcal{H}_{\mathrm{eff}}(\boldsymbol{S})/T]. \tag{11}$$

Thermodynamics follows from Eq. (11) as usual. The free energy, $\mathcal{F}$, and the electron density, x, are given by:

$$\mathcal{F}=-\frac{T}{V}\ln\mathcal{Z}_{\mathrm{GC}} \tag{12}$$

$$x=\frac{\partial\mathcal{F}}{\partial\mu}=\int dE\langle g(E;\boldsymbol{S})\rangle\frac{1}{1+\exp[(E-\mu)/T]}, \tag{13}$$

where $\langle\cdots\rangle$ stands for spectation value over equilibrium spin configurations.

The variational mean-field approach consists of comparing the actual system with a set of simpler reference models, whose Hamiltonians, $\mathcal{H}_{\boldsymbol{h}}$, depend on external parameters, $\boldsymbol{h}_i$. For simplicity, we choose the model:

$$\mathcal{H}_{\boldsymbol{h}}=-\sum_i\boldsymbol{h}_i\cdot\boldsymbol{S}_i. \tag{14}$$

The variational method is based on the inequality

$$\mathcal{F}\leqslant\mathcal{F}_{\boldsymbol{h}}+\langle\mathcal{H}^{\mathrm{eff}}-\mathcal{H}_{\boldsymbol{h}}\rangle_{\boldsymbol{h}}, \tag{15}$$

where $\mathcal{F}_{\boldsymbol{h}}$ is the free energy of the system with Hamiltonian (14), and the expectation values $\langle\cdots\rangle_{\boldsymbol{h}}$ are calculated with the Hamiltonian $\mathcal{H}_{\boldsymbol{h}}$. The inequality (15) follows easily from the concavity of the exponential function.[23] The best approximation to the actual free energy with the *ansatz* of Eq. (14) is

$$\mathcal{F}=\min_{\boldsymbol{h}}\{\mathcal{F}_{\boldsymbol{h}}+\langle\mathcal{H}^{\mathrm{eff}}\rangle_{\boldsymbol{h}}-\langle\mathcal{H}_{\boldsymbol{h}}\rangle_{\boldsymbol{h}}\}. \tag{16}$$

Since, for technical reasons that will become clear in the following, it is not possible to work with one field $\boldsymbol{h}_i$ per site, we must select some subsets that contain only a few independent parameters (see Sec. VII). The choice is of paramount importance since it is an *ansatz* that will artificially restrict the behavior of the system. We have chosen the following four families[30] of fields, depending on a parameter, $\boldsymbol{h}$:

$$\boldsymbol{h}_i=\boldsymbol{h}, \tag{17}$$

$$\boldsymbol{h}_i=(-1)^{z_i}\boldsymbol{h}, \tag{18}$$

$$\boldsymbol{h}_i=(-1)^{x_i+y_i}\boldsymbol{h}, \tag{19}$$

$$\boldsymbol{h}_i=(-1)^{x_i+y_i+z_i}\boldsymbol{h}, \tag{20}$$

which correspond, respectively, to FM, *A*-AFM, *C*-AFM, and *G*-AFM orderings. There is an order parameter (magnetization) associated to each of these orderings. We will denote them by M_{F}, M_{A}, M_{C}, and M_{G}, respectively. As a shorthand, they will be denoted generically by $\mathcal{M}$. The order parameter is related to the corresponding $\boldsymbol{h}$ by

$$\mathcal{M}=\frac{1}{\tanh h}-\frac{1}{h}, \tag{21}$$

where $h=|\boldsymbol{h}|/T$. Thus, the free energy can be written in terms of $\mathcal{M}$ instead of h and Eq. (16) implies that it must be minimized with respect to $\mathcal{M}$. The free energy has three contributions: the fermion free energy (FFE), the superexchange energy, and the entropy of the spins:

$$\mathcal{F}(\mathcal{M})=\mathcal{F}_{\mathrm{Fer}}(\mathcal{M})+NJ_{\mathrm{AF}}\mathcal{M}^2-T\mathcal{S}_{\boldsymbol{h}}(\mathcal{M}), \tag{22}$$

where N is, respectively, 3, -3, 1, and -1 for FM, *G*-AFM, *A*-AFM, and *C*-AFM orderings.

The entropy of the spins can be easily computed in terms of the mean field:

$$\mathcal{S}_{\boldsymbol{h}}(\mathcal{M}) = (\mathcal{F}_{\boldsymbol{h}} - \langle \mathcal{H}_{\boldsymbol{h}} \rangle_{\boldsymbol{h}})/T = \ln[\sinh h(\mathcal{M})/h(\mathcal{M})] - h(\mathcal{M})\mathcal{M}, \quad (23)$$

but the FFE,

$$\mathcal{F}_{\mathrm{Fer}}(\mathcal{M}) = -T \int dE \langle g(E;\boldsymbol{S}) \rangle_{\boldsymbol{h}} \ln[1 + \mathrm{e}^{-(E-\mu)/T}], \quad (24)$$

must be estimated numerically.

The nontrivial part of the computation is the average of the DOS $\langle g(E;\boldsymbol{S}) \rangle_{\boldsymbol{h}}$. The key is that it can be computed by numerical simulations on large lattices with high accuracy, due to two basic facts: (1) the mean-field Hamiltonian (14) describes uncorrelated spins and therefore equilibrium spin configurations can be easily generated on very large lattices, and (2) the DOS is a self-averaging quantity. This last point means that the mean value of the DOS can be obtained on a large lattice by averaging it over a small set of equilibrium configurations. Once the DOS is computed, the integral of Eq. (24) can be performed numerically to get the FFE as a function of $\mathcal{M}$.

IV. COMPUTATION OF THE AVERAGED DOS

The DOS can be accurately computed for *any* given spin configuration with the technique that we describe in the following.[21] From its definition, Eq. (9), the DOS is a probability distribution in the variable E, whose moments are

$$\mu_k(\boldsymbol{S}) = \int dE\, g(E;\boldsymbol{S}) E^k = \frac{1}{V} \mathrm{Tr}\, \mathcal{T}^k. \quad (25)$$

Now, it is easy to show that the eigenvalues of the hopping matrix verify $-6t \leq E_n < 6t$. A probability distribution of compact support can be reconstructed from its moments using the techniques of Stieljes.[31] In practice, we only know the first p moments, but the method of Stieljes allows us to find a good approximation to the distribution if p is large enough.

To compute the averaged DOS we follow four steps:

(i) Generate spin configurations, $\{\boldsymbol{S}\}$, according to the mean-field Boltzmann weight, $\exp(-\mathcal{H}_{\boldsymbol{h}}/T)$. This can be achieved very efficiently with a heat bath algorithm, since all the spins are decoupled in the mean-field Hamiltonian. In this way, one obtains spin configurations in perfect thermal equilibrium with the Boltzmann weight given by the mean-field Hamiltonian.

(ii) For each $\{\boldsymbol{S}\}$, one would calculate the moments of the DOS, using Eq. (25), and then apply the techniques of reconstruction of Stieljes.[31] However, this is impractical since, although the matrix $\mathcal{T}$ is sparse, the trace in Eq. (25) would require to repeat the process V times, and we would end up with an algorithm of order V^2. We use instead a stochastic estimator. First, we extract a normalized random vector $|v\rangle$, with components

$$v_i = \frac{\alpha_i}{\sum_{j=0}^{V} \alpha_j^2}, \quad (26)$$

where the α_i are random numbers extracted with uniform probability between -1 and 1. Let us now call $|n\rangle$ to the eigenvector of eigenvalue E_n of the matrix $\mathcal{T}$. It is easy to check that (the overline stands for the average on the random numbers α_i)

$$\overline{v_i v_j} = \frac{\delta_{i,j}}{V}, \quad (27)$$

$$\overline{\langle n|v\rangle\langle v|m\rangle} = \frac{\delta_{n,m}}{V}. \quad (28)$$

Then we introduce a v-dependent density of states:

$$g(E;v;\boldsymbol{S}) \equiv \sum_{n=1}^{V} |\langle n|v\rangle|^2 \delta(E - E_n). \quad (29)$$

From Eq. (28), it follows immediately that

$$\overline{g(E;v;\boldsymbol{S})} = g(E;\boldsymbol{S}). \quad (30)$$

From $\langle v|v\rangle = 1$, and from Eq. (29), we see that $g(E;v;\boldsymbol{S})$ is a perfectly reasonable distribution function, whose moments are

$$\int dE\, E^k g(E;v;\boldsymbol{S}) = \langle v|\mathcal{T}^k|v\rangle. \quad (31)$$

Numerically, the algorithm is of order $k \times V$, since, as mentioned, $\mathcal{T}$ is sparse and only $O(V)$ operations are required to multiply v by $\mathcal{T}$. This method allows us to compute a large number of moments on large lattices. However, notice that the actual calculation is not performed this way (round-off errors would grow enormously with the power of $\mathcal{T}$), but as explained in the Appendix.

(iii) Reconstruct $g(E;v;\boldsymbol{S})$ from the moments, by the method of Stieljes. The DOS is obtained in a discrete but very large number of energies, E. The cost of refining this set of energies is negligible. Hence, the integral over E that gives the FFE, Eq. (24), can be approximated numerically with high accuracy.

(iv) Average $g(E;v;\boldsymbol{S})$ over the spin configurations $\boldsymbol{S}$ and over the random vectors $|v\rangle$. In practice we only use a random vector per spin configuration: it is useless to obtain an enormous accuracy on the density of states for a particular spin configuration, that should be spin averaged, anyway. Since the errors due to the fluctuations of the spins and the fluctuations of the $|v\rangle$ are statistically uncorrelated, both of them average out simultaneously.[32] It is crucial that the DOS is a self-averaging quantity, what means that its fluctuations are suppressed as $1/\sqrt{V}$. Hence, its average over a few equilibrium configurations is enough to estimate it with high accuracy.

This program can be carried out successfully on lattices as large as 64^3 and even 96^3, computing a large enough number of moments, 50 or 75. As we shall see, this suffices to achieve an excellent accuracy in the averaged DOS and in the FFE.

The whole process is repeated for several values of the mean fields $\boldsymbol{h}$ within each family. The FFE computed in a

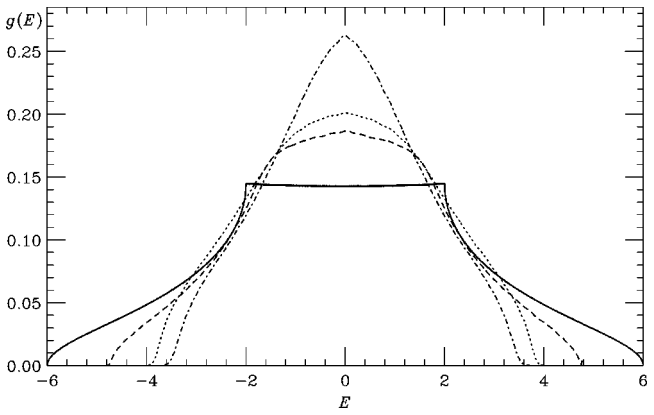

FIG. 1. Averaged DOS, reconstructed with 50 moments, versus E, for four values of the mean field corresponding to $M_F=1$ (solid line), $M_F=0.5$ (dashed line), paramagnetic (dotted line), and $M_G=0.5$ (dot-dashed line).

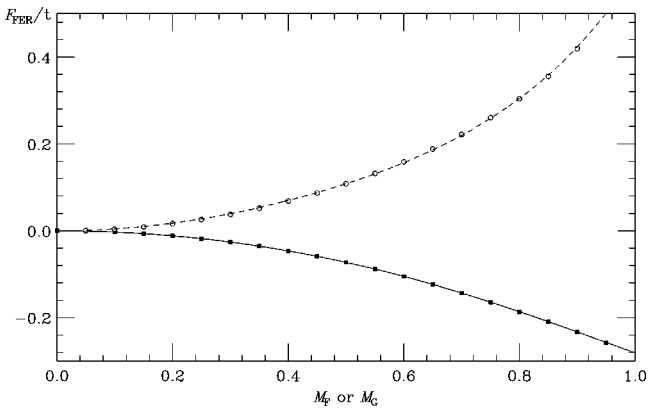

FIG. 2. FFE at $T=0$ and $\mu=0$ ($x=1/2$) versus M_F (squares, solid line) or M_G (circles, dotted line). The points are the results of the simulation and the lines are the three parameter fit.

discrete set of magnetizations is extended to a continuous function of $\mathcal{M}$ in the interval $[0,1]$ through a polynomial fit, as we will show in the next section. The magnetic phase diagram of the model will come out easily then.

V. EXTRACTING THE FERMIONIC FREE ENERGY

Let us discuss in this section the numerical results for the averaged DOS and the FFE. We carried out the program designed in the previous section for 20 values of $\boldsymbol{h}$ within each family of mean fields, chosen in such a way that the corresponding *magnetizations*, $\mathcal{M}$, are uniformly distributed in $[0,1]$. The expectation value $\langle g(E;\boldsymbol{S})\rangle_{\boldsymbol{h}}$ is estimated by averaging over 50 equilibrium (with respect to the mean-field distribution) spin configurations. This is enough to have the statistical errors under control on a 64^3 lattice.

Figure 1 displays the averaged DOS, computed on a 64^3 lattice for four values of $\boldsymbol{h}$, corresponding to FM ($M_F=0.5$ and $M_F=1$), paramagnetic, and G-AFM ($M_G=0.5$) phases. They were reconstructed with its 50 first moments.[33] Note that the DOS is even in E, as required by the particle-hole symmetry, and that it becomes narrower in going from the FM to the G-AFM phase, as expected. The width of the density of states in the PM phase is $8t$, two thirds of the width corresponding to the perfect ferromagnetic, in agreement with the results of full diagonalization.[34]

From the averaged DOS it is straightforward to compute the FFE by performing the integral entering Eq. (24) numerically. In this way, we computed $\mathcal{F}_{\rm Fer}$ for the chosen values of $\mathcal{M}$. Given that the free energy can be shifted by a term independent of $\mathcal{M}$, we use $\mathcal{F}_{\rm Fer}(\mathcal{M})-\mathcal{F}_{\rm Fer}(0)$ instead of $\mathcal{F}_{\rm Fer}(\mathcal{M})$.[35]

To have an analytic expression for $\mathcal{F}_{\rm Fer}$, we fit the data with a polynomial of order sixth in $\mathcal{M}$, with coefficients that depend on T and μ:

$$\mathcal{F}^{(I)}_{\rm Fer}(M_I)=A^{(I)}_2 M_I^2+A^{(I)}_4 M_I^4+A^{(I)}_6 M_I^6. \qquad (32)$$

The index I denotes the type of ordering: $I=$F, A, C, or G.

Figure 2 shows the FFE at $T=0$ and $\mu=0$, which corresponds to half filling, $x=1/2$, as a function of M_F or M_G. The points are the result of the numerical computation and the lines are the best fits of the form (32). The high quality of the fits is remarkable. Note that the fermions favor FM order. The coefficients $A^{(I)}_j(T,\mu)$ of Eq. (32), which will play a major role in the exploration of the phase diagram, are displayed in Fig. 3 in the cases $I=$F, G, for $T=0$, as a function of μ. We always found $A^{(F)}_2(T,\mu)<0$ and $A^{(G)}_2(T,\mu)>0$, in agreement with the FM nature of the spin interaction induced by the double exchange mechanism.

Let us estimate the errors of our numerical approach. We have three sources of errors: (a) The finite size of the lattice, (b) statistics, arising from the numerical simulation, and (c) truncation of the infinite sequence of moments.

Finite-size errors have been estimated comparing the results on a 64^3 and a 96^3 lattice. They turn out to be negligible, as expected given the sizes of the lattices. To estimate the statistical errors we performed three different simulations using the 50 lowest-order moments. One more simulation,

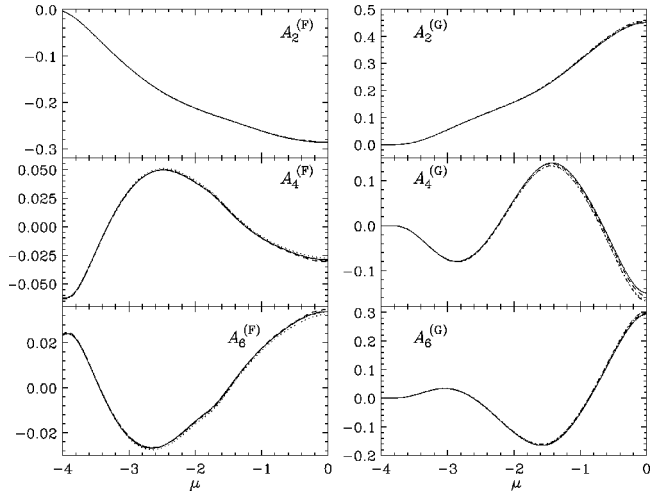

FIG. 3. Coefficients $A^{(F)}_2$, $A^{(G)}_2$, $A^{(F)}_4$, $A^{(G)}_4$, $A^{(F)}_6$, and $A^{(G)}_6$ of the fits (32) versus μ, at $T=0$. Each figure contains four lines (that sometimes cannot be distinguished) corresponding to the four different computations mentioned in the text, three with 50 and one with 75 moments.

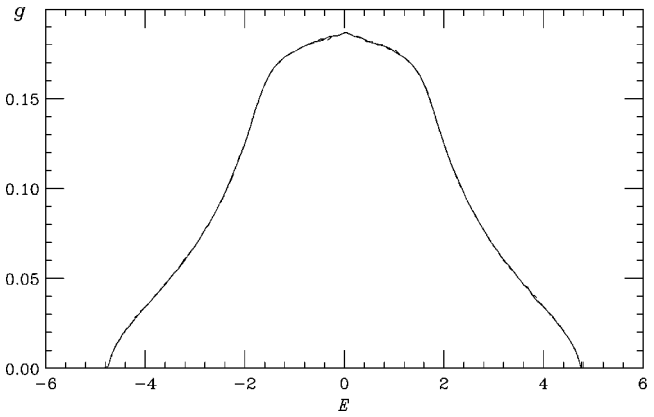

FIG. 4. Averaged DOS vs energy for $M_F=0.5$ on a 64^3 lattice from a simulation using 50 moments (solid line) and another one with 75 moments (dashed). The curves can hardly be distinguished on this scale.

this time with the 75 first moments, was done in order to study the systematic error associated to the truncation of the sequence of moments. As an example, Fig. 4 displays the averaged DOS in the FM phase ($M_F=0.5$) extracted from two different simulations, one with 50 and the other with 75 moments. We see only tiny differences, which can hardly be appreciated on the scale of the figure. This small error propagates to the FFE, which is shown in Fig. 5 for $T=0$ and $\mu=0$. There are four sets of points plotted, corresponding to the four mentioned simulations. Again, the differences cannot be appreciated. The errors in the computed FFE give rise to uncertainties in the coefficients A of Eq. (32), which can be appreciated in Fig. 3. The largest errors appear at $\mu=0$ (half filling). We have also checked that fits to a polynomial of an eight order do not change the values of $A_j^{(I)}$ significantly.

To summarize, we have checked that the numerical uncertainties inherent to our numerical approach are well under

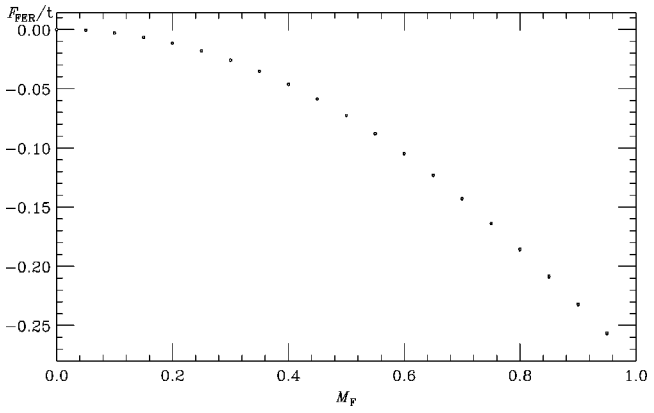

FIG. 5. Fermion free energy vs M_F from four simulations on a 64^3 lattice. Three of them, carried out to estimate the statistical errors, used 50 moments to reconstruct the DOS. The other one, aimed to estimate the systematic errors due to the truncation of the sequence of moments, took into account 75 moments. The errors turn out to be so small that they cannot be appreciated on the scale of the figure.

control and therefore all the conclusions are robust in this sense. The discrepancies between our analysis and the true behavior of the system, if they are important, must be attributed *only* to the mean-field *ansatz*.

VI. EFFECT OF THE BERRY PHASE

The role of the Berry phase in the effective hopping term, in the doping range studied here, has not been investigated. It has been established, however, that Berry phases associated with orbital rotations in the two-dimensional $\mathbf{e}_g$ subspace can lead to the stabilization of phases with orbital ordering for dopings $x \geqslant 0.5$.[26,36] At intermediate dopings, however, it is known that cubic symmetry is restored by the double exchange interaction, and there is no static Jahn-Teller distortion. On theoretical grounds, an orbital wave at these fillings must have a long wavelength in order to open gaps at the Fermi surface. Such an instability should be very sensitive to disorder, and the associated energy gain is probably smaller than that induced by other instabilities. Hence, for $0.1 \leqslant x \leqslant 0.5$ we do not expect the degeneracy between the two $\mathbf{e}_g$ orbitals to be broken, and we do not need to consider the associated Berry phase. An intriguing possibility, however, is the breaking of the orbital degeneracy in such a way that the material retains the full cubic symmetry.[27] In this case, no orbital Berry phase is induced.

In the following, we elucidate the role of the Berry phase associated with rotations in spin space, which can be important even in the absence of orbital ordering. To investigate this point, let us repeat our analysis of the DEM setting the Berry phase to zero. All we have to do is to compute the DOS of the hopping matrix $\mathcal{T}_{ij}^{\text{mod}}$ of Eq. (5). The rest is identical to what we have discussed in the previous sections.

Figure 6 displays the averaged DOS at $M_F=0$ (PM phase) and $M_F=0.5$ for hopping with and without the Berry phase. At first sight, the differences, although noticeable (they are much bigger than the errors, cf. Fig. 4), do not seem very important. However, it happens that the results are very sensitive to small modifications of the DOS. We shall see indeed that the presence or absence of the Berry phase is crucial for some features of the phase diagram. Thus, the analysis of errors of the previous section turns out to be extremely important to give a meaning to our results. Notice that the effect of the Berry phase is stronger in the disordered phase, as expected.

Figure 7 shows the effects of the Berry phase on the FFE at $T=0$ and $\mu=0$. These effects modify the coefficients $A_k^{(I)}$ entering $\mathcal{F}_{\text{Fer}}$, which can be seen in Fig. 8. These coefficients are very sensitive to the modifications of the DOS induced by the Berry phase. Of special relevance is $A_4^{(F)}$, which, as we shall see in the next section, governs the possibility of having first-order PM-FM transitions. In particular, in the vicinity of $\mu=0$ this coefficient is negative. Notice, however, that without the Berry phase $A_4^{(I)}$ is negative around $\mu=0$ in a smaller region than with Berry phase, and it is closer to zero. This fact induces important differences in the nature of the phase transitions of the model, as we shall see in the next section.

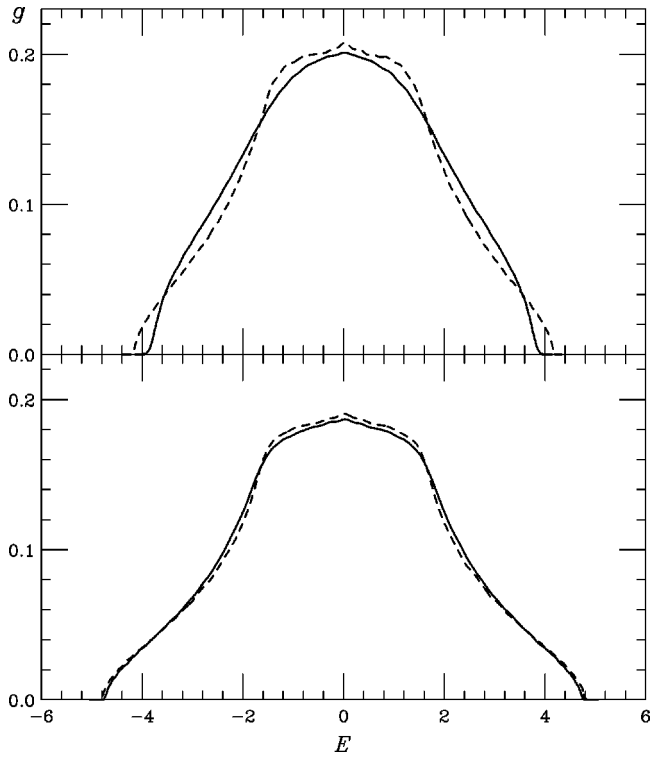

FIG. 6. Averaged DOS in the paramagnetic phase ($M_F=0$, upper panel) and in the ferromagnetic phase ($M_F=0.5$, lower panel) with (solid) and without (dashed) Berry phase.

VII. PHASE DIAGRAM

The equilibrium states are determined by the absolute minima of the free energy, Eq. (22), with respect to the order parameters, $\mathcal{M}$. The minima determine the phases and the phase boundaries. Given that we know $\mathcal{F}$ as a function of $\mathcal{M}$, the problem of determining the equilibrium states is reduced to numerical minimization of a function of a single variable. This is indeed the way we proceed. It is, however,

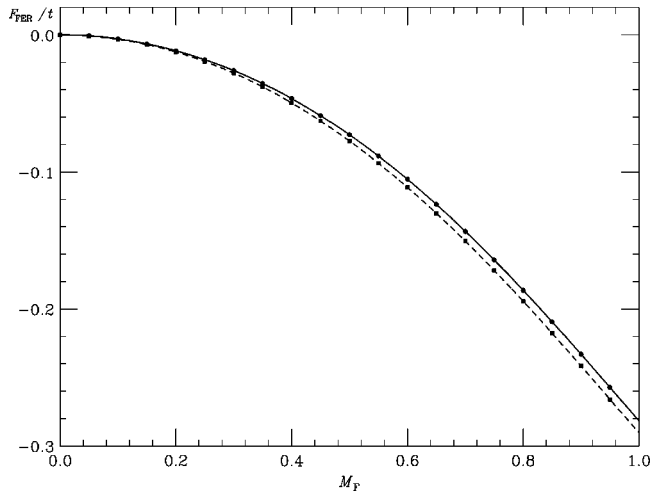

FIG. 7. Fermion free energy at $T=0$ and $\mu=0$ as a function of M_F with (solid) and without (dashed) Berry phase. Notice that, in both cases, the free energy has been taken vanishing at the origin by convention.

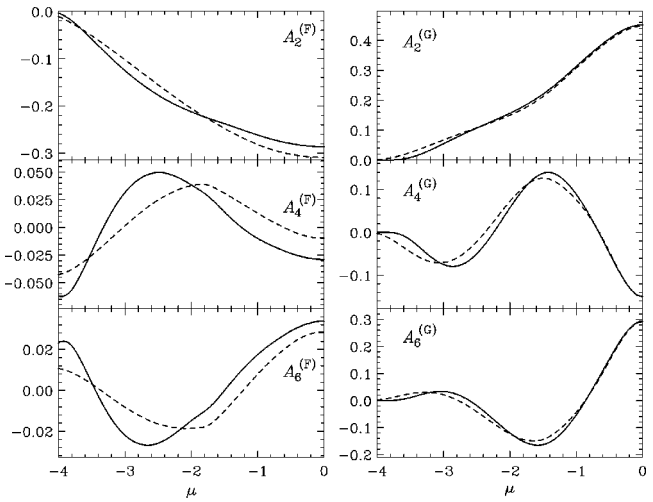

FIG. 8. Coefficients of the fit (32) of the fermion free energy at $T=0$ as a function of μ with (solid) and without (dashed) Berry phase.

illuminating to get some insight by a semianalytic treatment of the problem. As we have seen, to a very good approximation, the FFE is a polynomial of sixth degree in $\mathcal{M}$. The entropy (23) can also be expanded in powers of $\mathcal{M}$ around $\mathcal{M}=0$:

$$\mathcal{S}_h(\mathcal{M})=-\left(\frac{3}{2}\mathcal{M}^2+\frac{9}{20}\mathcal{M}^4+\frac{99}{350}\mathcal{M}^6+\cdots\right). \quad (33)$$

Hence, we find the Landau expansion of the free energy in powers of the order parameter.

$$\mathcal{F}(\mathcal{M})=c_2\mathcal{M}^2+c_4\mathcal{M}^4+c_6\mathcal{M}^6+\cdots. \quad (34)$$

The coefficients of the expansion are

$$c_2=\frac{3}{2}T+NJ_{\mathrm{AF}}+A_2^{(I)}(T,\mu), \quad (35)$$

$$c_4=\frac{9}{20}T+A_4^{(I)}(T,\mu), \quad (36)$$

$$c_6=\frac{99}{350}T+A_6^{(I)}(T,\mu), \quad (37)$$

where N was defined right after Eq. (22).

The free energy has the symmetry $\mathcal{M}\rightarrow-\mathcal{M}$. At high T, the entropic term dominates and the minimum of $\mathcal{F}$ is at $\mathcal{M}=0$. As the temperature decreases, the internal energy becomes more important and the absolute minimum of $\mathcal{F}$ can be located at $\mathcal{M}\neq0$. The phase transition will be *continuous* when the absolute minimum at the origin changes to a maximum, i.e.:

$$c_2=0\Rightarrow\frac{3}{2}T_c+NJ_{\mathrm{AF}}+A_2^{(I)}(T_c,\mu)=0. \quad (38)$$

At a *first-order transition* three minima, $\mathcal{M}=0$ and $\mathcal{M}=\pm\mathcal{M}_0\neq0$, are degenerate. Three conditions must hold:

(i) Minimum at $\mathcal{M}=0$:

$$c_2>0. \tag{39}$$

(ii) Minimum at $\mathcal{M}_0$:

$$2c_2+4c_4\mathcal{M}_0^2+6c_6\mathcal{M}_0^4=0. \tag{40}$$

(iii) Degeneracy $[\mathcal{F}(0)=\mathcal{F}(\mathcal{M}_0)]$:

$$c_2+c_4\mathcal{M}_0^2+c_6\mathcal{M}_0^4=0. \tag{41}$$

The solution of these three equations is

$$\mathcal{M}_0^2=-2c_2/c_4, \tag{42}$$

$$c_6=c_4^2/(4c_2), \tag{43}$$

$$c_2>0; \quad c_4<0; \quad c_6>0. \tag{44}$$

Equation (42) gives the spontaneous magnetization; Eq. (43) determines the critical temperature T_c of the first-order transition as a function of μ and J_{AF}; Eq. (44) sets necessary conditions (real $\mathcal{M}_0$) for a first-order transition to happen. We see that to have a first-order PM-FM transition we must have $A_4^{(I)}(T_c,\mu)<0$. Figure 3 shows that in particular this is possible around half filling.

The boundaries between first- and second-order lines are tricritical points. They are determined by the conditions:

$$c_2=0\Rightarrow J_{AF}^t=-\frac{3}{2N}T_t-\frac{A_2^{(I)}(T_t,\mu)}{N}, \tag{45}$$

$$c_4=0\Rightarrow T_t=-\frac{20}{9}A_4^{(I)}(T_t,\mu). \tag{46}$$

With these ingredients, we are able to discuss the phase diagram of the DEM. It has been shown in Ref. 20 that the phase diagram of double exchange systems is richer than previously anticipated and differs substantially from that of more conventional itinerant ferromagnets. Moreover, it is consistent with the magnetic properties of manganites[8–13,37–39] (see Sec. IX).

We shall not repeat here the analysis of the phase diagram of the DEM carried out in Ref. 20. Let us concentrate on the effects of the Berry phase. Figure 9 displays the phase diagram in the plane $(x,T/t)$, for several values of J_{AF}. The left part corresponds to the model that includes the Berry phase and on the right the Berry phase is neglected. For $J_{AF}<0.06$ both phase diagrams are very similar. The transition temperature is slightly higher (13%) at half filling in the model that ignores the Berry phase. At low filling, both phase diagrams are almost identical. However, for $J_{AF}>0.06$ important differences arise. A first-order PM-FM transition develops around half filling if the Berry phase is taken into account. The onset for such behavior is $J_{AF}=0.06$. In contrast, the PM-FM transition around half filling remains continuous for any value of J_{AF} if the Berry phase is neglected. The explanation is simple: the coefficient $A_4^{(F)}$, although negative, has too small an absolute value to drive a first-order transition. This negative coefficient would become

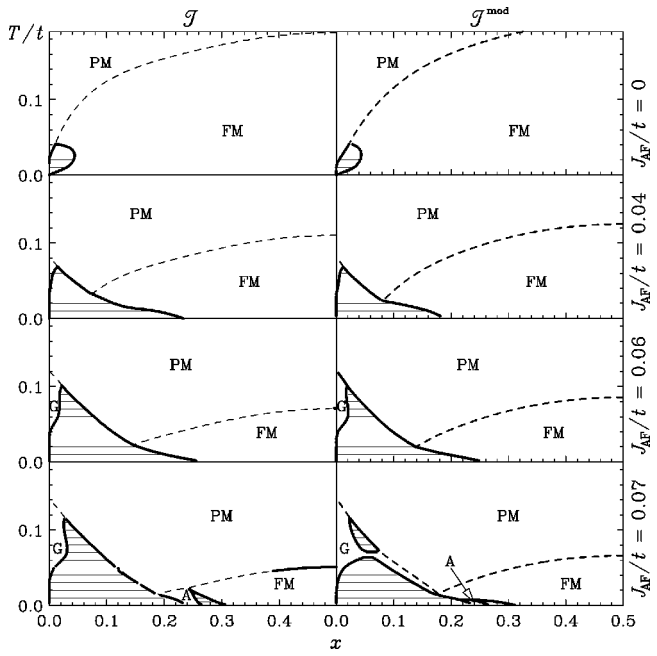

FIG. 9. Phase diagram of the DEM in the plane $(x,T/t)$, for several values of J_{AF}/t. The left (right) part corresponds to the model with (without) Berry phase. Solid (dashed) lines represent first- (second-) order transitions and the zones with stripes are phase-separation regions. The onset for first-order PM-FM transition is at $J_{AF}\approx 0.06$ in the model with Berry phase, while such transitions do not appear if the Berry phase is neglected.

effective if the critical temperature were much lower, which can be achieved by increasing the AF superexchange coupling. But in this case the competition between FM and AF is so strong that the transition at half filling takes place between PM and A-AFM phases, and it is second order. First-order PM-FM transitions only appear if the Berry phase is properly taken into account.

At $T=0$, the phase diagrams are similar in both cases, and we only display that of the model without Berry phase in Fig. 10. The discussion of Ref. 20 applies to this case with-

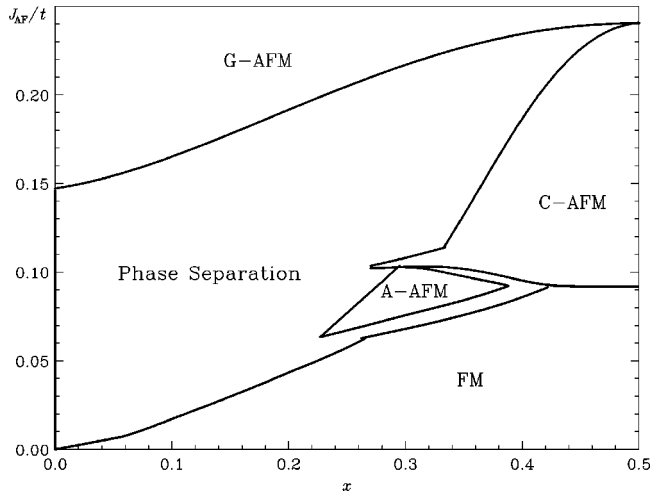

FIG. 10. Phase diagram of the DEM without Berry phase in the plane (x,J_{AF}) at $T=0$.

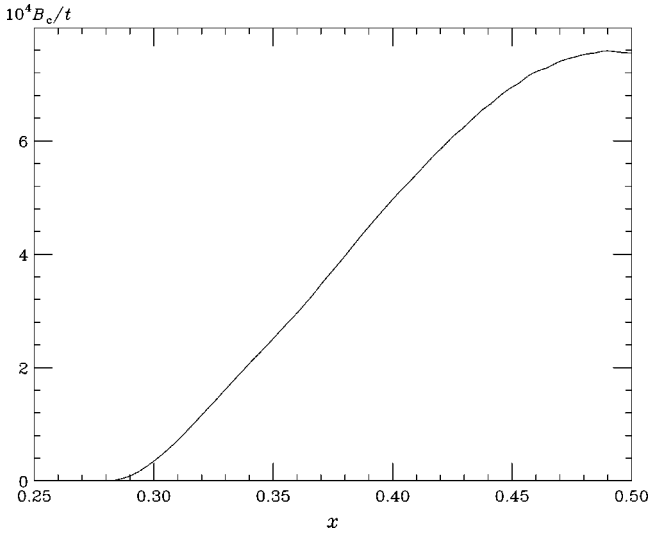

FIG. 11. Critical magnetic field (in units of $10^{-4}\,t$) versus x at $J_{\rm AF}=0.08\,t$.

out any modification.

Let us end this section with the analysis of the phase transitions at finite applied magnetic field, B. The first-order PM-FM transition around half filling survives under an applied magnetic field. In this case, the order parameter, $M_{\rm F}$, is nonzero in both phases, but suffers a jump on a line in the plane (B,T). The line ends at a critical point, (B^*,T^*), which has a certain magnetization $M_{\rm F}^*$. The critical field can be measured and is of interest.[40,41] Let us compute it. The free energy in the presence of a magnetic field, B, is

$$\mathcal{F}(M_{\rm F})=c_2M_{\rm F}^2+c_4M_{\rm F}^4+c_6M_{\rm F}^6-BM_{\rm F}. \tag{47}$$

The magnetic field shifts the three degenerate minima of the zero-field PM-FM first-order transition and lifts the degeneracy. By tuning (increasing) the temperature it is possible to get two degenerate minima again, and a first-order transition takes place. In this way, we get a transition line in the (B,T) plane. Increasing B, the two degenerate minima become closer. At the critical field, B^*, both minima coalesce at some point $M_{\rm F}^*$, and the transition disappears. When this happens, the three first derivatives of $\mathcal{F}$ in respect to $M_{\rm F}$ vanish, and the fourth is positive. These conditions read

$$\mathcal{F}'(M_{\rm F}^*)=0\Rightarrow B^*=2c_2M_{\rm F}^*+4c_4M_{\rm F}^{*3}+6c_6M_{\rm F}^{*5}, \tag{48}$$

$$\mathcal{F}''(M_{\rm F}^*)=0\Rightarrow 2c_2+12c_4M_{\rm F}^{*2}+30c_6M_{\rm F}^{*4}=0, \tag{49}$$

$$\mathcal{F}'''(M_{\rm F}^*)=0\Rightarrow 24c_4M_{\rm F}^*+120c_6M_{\rm F}^{*3}=0, \tag{50}$$

$$\mathcal{F}^{(iv)}(M_{\rm F}^*)>0\Rightarrow 24c_4+360c_6M_{\rm F}^{*2}>0. \tag{51}$$

These equations determine B^*, $T_{\rm c}$, and $M_{\rm F}^*$ as a function of μ (or x) and $J_{\rm AF}$. The critical temperature $T_{\rm c}$ varies very little from its value at $B=0$. Figure 11 displays B^*, in units of $10^{-4}\,t$, versus x, for $J_{\rm AF}=0.08\,t$. In physical units, using $t\approx 0.166$ eV, B^* varies from 0.6 T at $x=0.33$ to 2.2 T at $x=0.5$. Recent measurements in $La_{0.6}Y_{0.07}Ca_{0.33}MnO_3$ gave a critical field of 1.5 T.[41]

VIII. COMPARISON WITH OTHER CALCULATIONS

A. Rigid band mean field approximation

The main conclusion of the variational mean-field technique applied to the DEM is the prediction of a first-order PM-FM transition at half filling and its vicinity for $J_{\rm AF}/t \in [0.06,0.1]$. This is in sharp contrast with the widely used mean-field approach devised by de Gennes in 1960,[14] which predicts a second-order PM-FM at half filling for any value of $J_{\rm AF}$. Let us see briefly what are the differences between these two approaches that yield different qualitative behavior.

The difficulty in the mean-field approach to the DEM lies in calculating the contribution of the fermions to the mean-field free energy. In the variational method discussed here, we compute it exactly through a numerical simulation. As we have already mentioned, the only approximation is the mean-field *ansatz* for the Boltzmann weights of the spin configurations. On the other hand, de Gennes suggested that the fermion free energy might be well approximated by the free energy of an assembly of fermions propagating on a crystal with a homogeneous hopping parameter given by the average of the spin-dependent hopping parameter over the mean-field spin configurations. The de Gennes' method neglects the influence of the Berry phase. In this approach, the electronic DOS depends on the spin configuration only through the hopping parameter (in this case, without the Berry phase): $g(E;\boldsymbol{S})=g[E;\mathcal{T}^{\rm mod}(\boldsymbol{S}_i\cdot\boldsymbol{S}_j)]$. In mathematical terms, de Gennes' approximation is carried out through the following substitution:

$$\begin{aligned}\langle g(E;|\mathcal{T}(\boldsymbol{S}_i\cdot\boldsymbol{S}_j)|)\rangle_{\boldsymbol{h}}&\rightarrow g(E;\langle|\mathcal{T}(\boldsymbol{S}_i\cdot\boldsymbol{S}_j)|\rangle_{\boldsymbol{h}})\\&=g_0(E;\mathcal{T}_0),\end{aligned} \tag{52}$$

where $g_0(E;\mathcal{T}_0)$ is the DOS of free fermions with hopping

$$\begin{aligned}\mathcal{T}_0(h)&=\langle|\mathcal{T}(\boldsymbol{S}_i\cdot\boldsymbol{S}_j)|\rangle_{\boldsymbol{h}}\\&=-\frac{2}{J_{1/2}^2(-{\rm i}h)}\sum_{l=0}^{\infty}\frac{J_{l+1/2}^2(-{\rm i}h)}{(2l-1)(2l+3)},\end{aligned} \tag{53}$$

and $J_\nu(z)$ is the Bessel function.

Since the hopping is homogeneous, the fermion free energy is known analytically. At $T=0$ and half filling ($\mu=0$) it is

$$\mathcal{F}_{\rm Fer}=\int_{-\mathcal{T}_0W_0}^{0}dE\,g(E;\mathcal{T}_0)E \tag{54}$$

$$=-\mathcal{T}_0(h)\int_0^{W_0}dE\,g_0(E;1)E. \tag{55}$$

All the dependence in the magnetization is contained in $\mathcal{T}_0(\boldsymbol{h})$. The expansion in powers of the magnetization follows straightforwardly from Eqs. (53) and (21). It yields:

$$\frac{1}{t}\mathcal{T}_0(h(M_{\rm F}))=\frac{2}{3}+\frac{2}{5}M_{\rm F}^2-\frac{6}{175}M_{\rm F}^4-\frac{18}{875}M_{\rm F}^6+\cdots . \tag{56}$$

The coefficient of $M_{\rm F}^4$ in $\mathcal{F}_{\rm Fer}$ is *positive*. Hence, the PM-FM phase transition at half filling can only be continuous. We have also checked that this remains true when we keep the contribution of all powers of $M_{\rm F}$ to $\mathcal{F}_{\rm Fer}$.

The fermions in de Gennes's approach propagate only on perfect crystals. In the truly variational mean-field presented in this work, the fermions propagate on the disordered spin background generated by the mean field $\boldsymbol{h}$. This appears as an important ingredient that leads the predictions closer to the phenomenology, as we have shown in Ref. 20.

B. Dynamical mean field approximation

This method allows for an improvement on the treatment of the electronic contribution to the self-energy. In the PM phase, the density of states is proportional to that in the fully ferromagnetic phase, like in de Gennes treatment. The only difference is that the constant of proportionality is $1/\sqrt{2}$ and not 2/3. Below $T_{\rm c}$, the density of states is calculated self-consistently, through a self-energy which can be written as:

$$\Sigma(E;\boldsymbol{S}_i)=\langle|\mathcal{T}(\boldsymbol{S}_i\cdot\boldsymbol{S}_j)|^2 g(E;\boldsymbol{S}_j)\rangle_{\boldsymbol{S}_j} \tag{57}$$

and:

$$g(E;\boldsymbol{S}_i)=\frac{1}{E-\Sigma(E;\boldsymbol{S}_i)}. \tag{58}$$

Finally, the average $\langle\cdots\rangle_{\boldsymbol{S}_j}$ is carried out defining a probability distribution, $\mathcal{P}(\boldsymbol{S}_j)$, which depends self-consistently on the free energy associated with a site with magnetization $\boldsymbol{S}_j$ immersed in the lattice described by $\mathcal{P}(\boldsymbol{S}_j)$.

Our approach is similar to the dynamical-mean-field approximation, but differs from it in two aspects:

(i) The electronic density of states is calculated in a cubic lattice, instead of using the semielliptical DOS valid in the Bethe lattice with infinite coordination.

(ii) We use a variational *ansatz* for $\mathcal{P}(\boldsymbol{S}_j)$, instead of determining it fully self-consistently.

Point (i) allows us to consider effects of the lattice geometry, and the influence of the Berry phase, as discussed above. At zero temperature, where both approaches become exact for their respective lattices, we find phases which can only be defined in a 3D cubic lattice.

If the transition is continuous, the distribution $\mathcal{P}(\boldsymbol{S}_j)$ can be expanded on the deviation from the isotropic one, $\mathcal{P}(\boldsymbol{S}_j)=\text{const}$ in the PM phase. The *ansatz* that we use has the correct behavior sufficiently close to $T_{\rm c}$, so that both approaches will predict the same value of $T_{\rm c}$ for a given lattice. One must be more careful in the study of discontinuous transitions. Our *ansatz* introduces an approximation in the ordered phase (which disappears at $T=0$). However, near a first-order transition we do not expect divergent critical fluctuations, so that our approach should give qualitative, and probably semiquantitative correct results as compared to the DMFA, in lattices where the latter is exact.

C. Hierarchy of approximations

We are tempted to design a hierarchy of approximations, ordered according to the coefficient $A_4^{(\rm F)}$ of the $M_{\rm F}^4$ term in the Landau expansion of the fermion free energy, as follows:

(1) de Gennes's approximation: $A_4^{(\rm F)}>0$ and the PM-FM transition is second order.

(2) Exact variational computation without the Berry phase: $A_4^{(\rm F)}<0$ but $|A_4^{(\rm F)}|$ too small to produce first-order PM-FM transitions, see Eq. (36).

(3) Exact variational computation with the Berry phase: $A_4^{(\rm F)}<0$ and $|A_4^{(\rm F)}|$ large enough to produce first-order PM-FM transitions.

IX. CONCLUSIONS

We have presented a detailed analysis of the variational mean-field technique. This method can be useful in any situation where non-self-interacting fermions are coupled to classical continuous degrees of freedom. Within this method, the fermionic contribution to the free energy is calculated exactly, and, later on, the variational mean-field method is applied to the classical degrees of freedom. As an example, we have chosen the double exchange model, both with and without the Berry phase. The phase diagram has been obtained in both situations.

We have shown that the Berry phase is crucial in order to get first-order PM-FM phase transitions around half filling. Such transitions are second order if the topological effects associated to the Berry phase are neglected. Thus, the dimensionality of the lattice plays a very important role in the structure of the phase diagram.

Some earlier mean-field computations[14,19] approximate the fermion free energy by that of an assembly of fermions propagating on a perfect crystal with a homogeneous hopping parameter averaged over the spin configurations. They yield second order FM-PM transitions in the vicinity of half filling. The propagation of the fermions in the disordered spin background generated by the mean field is another crucial ingredient to get discontinuous PM-FM transitions at half filling. More modern approaches, such as the DMFA[25] cannot deal with three dimensional effects such as the Berry phase either.

As shown in Ref. 20, the variational mean field described in the present work leads to results that are consistent with the phenomenology of the magnetic properties of the manganites $La_{1-x}(Sr,Ca)_xMnO_3$, in the range $0.3\leqslant x\leqslant 0.5$, in particular with the fact that for materials with a high-transition temperature, the PM-FM transition is continuous while for those with low $T_{\rm c}$ it is not. Moreover, the order of magnitude of our estimate of the critical field for which histeretic effects disappear agrees with the experimental findings in $La_{0.60}Y_{0.07}Ca_{0.33}MnO_3$.[41] Also the phase diagram obtained by substitution of a trivalent rare earth for another one

with smaller ionic radius (i.e., compositional changes that do not modify the doping level) is in remarkable agreement with our results.

Of course, the DEM itself can also be highly improved. For instance, one should include the orbital degeneracy, which is known to play an important role, and other elements like phonons and Jahn-Teller distortions. The variational mean-field approach can be applied with the same techniques presented in this work whenever the bosonic fields that interact with the electrons can be treated as classical.

ACKNOWLEDGMENTS

We are thankful for helpful conversations to L. Brey, J. Fontcuberta, G. Gómez-Santos, C. Simon, J. M. de Teresa, and especially to R. Ibarra and V. S. Amaral. V.M.-M. was partially supported by MEC. We acknowledge financial support from Grant Nos. PB96-0875, AEN97-1680, AEN97-1693, AEN97-1708, AEN99-0990 (MEC, Spain), and (07N/0045/98) (C. Madrid).

APPENDIX: THE METHOD OF MOMENTS

In this appendix we include, for completeness, some details on the method of moments.[21] For a complete mathematical background we refer to Ref. 31. The method of moments allows to obtain some statistical properties of large matrices (as the density of states or the dynamical structure factors, in general quantities depending on two-legged Green functions), without actually diagonalizing the matrices. Regarding the density of states, once one recognizes that it is a probability function whose moments can be obtained by iteratively multiplying by $\mathcal{T}$ the initial random vector $|v\rangle$, it is clear that the classical Stieljes techniques[31] can be used. Owing to the fact that the matrix $\mathcal{T}$ is sparse, and using the random vector trick, Eq. (31), the moments can be calculated with order V operations. Since the spectrum of the matrix $\mathcal{T}$ lies between $-6t$ and $6t$ for any spin configuration, the Stieljes method is guaranteed to converge. The procedure is as follows: one first introduces the resolvent

$$R(z)=\int_{-6t}^{6t} dE' \frac{g(E')}{z-E'}, \tag{A1}$$

that has a cut along the spectrum of $\mathcal{T}$, with discontinuity

$$2\pi g(E)=\mathrm{Im}\lim_{\epsilon\to 0}[R(E-i\epsilon)-R(E+i\epsilon)]. \tag{A2}$$

The resolvent can be obtained from the orthogonal polynomials of the $g(E)$, with the monic normalization:

$$P_n(E)=E^n+C_{n-1}E^{n-1}+\cdots, \tag{A3}$$

$$\delta_{n,m}\propto\int_{-6t}^{6t} dE\, g(E)P_n(E)P_m(E), \tag{A4}$$

with $P_0=1$, $P_{-1}=0$, and $n,m=0,1,\ldots$. The polynomials verify the following recursion relation:

$$P_{n+1}(E)=(E-a_n)P_n(E)-b_nP_{n-1}(E), \tag{A5}$$

with the coefficients a_n and b_n given by

$$a_n=\frac{\int_{-6t}^{6t} dE\, g(E)E\,P_n^2(E)}{\int_{-6t}^{6t} dE\, g(E)P_n^2(E)}, \tag{A6}$$

$$b_n=\frac{\int_{-6t}^{6t} dE\, g(E)P_n^2(E)}{\int_{-6t}^{6t} dE\, g(E)P_{n-1}^2(E)}. \tag{A7}$$

The coefficient b_0 is arbitrary and is conventionally settled to one.

The resolvent has a representation in terms of a continued fraction as follows:

$$R(z)=\cfrac{1}{z-a_0-\cfrac{b_1}{z-a_1-\cfrac{b_2}{z-a_2-\cdots}}}. \tag{A8}$$

If one truncates the continued fraction, the resolvent would be approximated by a rationale function, which does not have a cut and use of Eq. (A2) is impossible. Fortunately, when, as in this case, the density of states does not have gaps, the coefficients a_n and b_n tend fastly to their asymptotic values a and b.[31] Thus, one can end the continued fraction[22] with a truncation factor $T(z)$, that verifies

$$T(z)=\frac{b}{z-a-T(z)}. \tag{A9}$$

Since the previous equation is quadratic in $T(z)$, we find that $T(z)$ has a branch cut between $a-2\sqrt{b}$ and $a+2\sqrt{b}$, which are the limits of the spectrum.

One should not use the moments of the $g(E)$ calculated with Eq. (31) to obtain the orthogonal polynomials (and hence the $\{a_n,b_n\}$), since this is an extremely unstable numerical procedure. It is better to use the recurrence relation:

$$P_{n+1}(\mathcal{T})|v\rangle=(\mathcal{T}-a_n)P_n(\mathcal{T})|v\rangle-b_nP_{n-1}(\mathcal{T})|v\rangle, \tag{A10}$$

starting with

$$P_{-1}(\mathcal{T})|v\rangle=0,\quad P_0(\mathcal{T})|v\rangle=|v\rangle. \tag{A11}$$

From this, one immediately gets

$$a_n=\frac{\langle P_n(\mathcal{T})v|\mathcal{T}P_n(\mathcal{T})v\rangle}{\langle P_n(\mathcal{T})v|P_n(\mathcal{T})v\rangle}, \tag{A12}$$

$$b_n=\frac{\langle P_n(\mathcal{T})v|P_n(\mathcal{T})v\rangle}{\langle P_{n-1}(\mathcal{T})v|P_{n-1}(\mathcal{T})v\rangle}. \tag{A13}$$

In this way, one generates the Nth orthogonal polynomial of the matrix (times v) recursively, at the price of N multiplications per $\mathcal{T}$. The cost of this procedure is always of order V operations. For each random vector, one first extracts the

density of states through Eq. (A2), which is subsequently averaged over the different $|v\rangle$ and spin realizations.

Let us finally point out that the above recursion relation is virtually identical to the Lanzcos method (the only difference lies on the normalizations). It should therefore not be pursued for a large number of orthogonal polynomials, without reorthogonalization. For the relative modest number of coefficients calculated in this work, this has not been needed.

[1] E.D. Wollan and W.C. Koehler, Phys. Rev. **100**, 545 (1955).
[2] D.I. Khomskii and G. Sawatzky, Solid State Commun. **102**, 87 (1997).
[3] J.M.D. Coey, M. Viret, and S. von Molnar, Adv. Phys. **48**, 167 (1999).
[4] C. Zener, Phys. Rev. **82**, 403 (1951).
[5] P.W. Anderson and H. Hasegawa, Phys. Rev. **100**, 675 (1955).
[6] A.J. Millis, P.B. Littlewood, and B.I. Shraiman, Phys. Rev. Lett. **74**, 5144 (1995).
[7] J. van den Brink, G. Khaliullin, and D. Khomskii, Phys. Rev. Lett. **83**, 5118 (1999); T. Mizokawa, D.I. Khomskii, and G.A. Sawatzky, Phys. Rev. B **61**, R3776 (2000).
[8] J.M. de Teresa, M.R. Ibarra, P.A. Algarabel, C. Ritter, C. Marquina, J. Blasco, J. García, A. de Moral, and Z. Arnold, Nature (London) **386**, 256 (1997).
[9] M. Uehara, S. Mori, C.H. Chen, and S.-W. Cheong, Nature (London) **399**, 560 (1999).
[10] M. Fäth, S. Freisem, A.A. Menovsky, Y. Tomioka, J. Aarts, and J.A. Mydosh, Science **285**, 1540 (1999).
[11] J. Fontcuberta, B. Martínez, A. Seffar, S. Piñol, J.L. García-Muñoz, and X. Obradors, Phys. Rev. Lett. **76**, 1122 (1996).
[12] J.A. Fernandez-Baca, P. Dai, H.Y. Hwang, C. Kloc, and S.-W. Cheong, Phys. Rev. Lett. **80**, 4012 (1998).
[13] J. Mira, J. Rivas, F. Rivadulla, C. Vazquez-Vazquez, and M.A. López-Quintela, Phys. Rev. B **60**, 2998 (1999).
[14] P.-G. de Gennes, Phys. Rev. **118**, 141 (1960).
[15] E.L. Nagaev, Physica B **230**, 816 (1997).
[16] J. Riera, K. Hallberg, and E. Dagotto, Phys. Rev. Lett. **79**, 713 (1997).
[17] D.P. Arovas and F. Guinea, Phys. Rev. B **58**, 9150 (1998).
[18] S. Yunoki, J. Hu, A.L. Malvezzi, A. Moreo, N. Furukawa, and E. Dagotto, Phys. Rev. Lett. **80**, 845 (1998).
[19] D. Arovas, G. Gómez-Santos, and F. Guinea, Phys. Rev. B **59**, 13 569 (1999).
[20] J.L. Alonso, L.A. Fernández, F. Guinea, V. Laliena, and V. Martin-Mayor, cond-mat/0003472, Phys. Rev. B (to be published); cond-mat/0007450, Nucl. Phys. B (to be published).
[21] C. Benoit, E. Royer, and G. Poussigue, J. Phys.: Condens. Matter **4**, 3125 (1992), and references therein; C. Benoit, *ibid.* **1**, 335 (1989); G. Viliani, R. DellÁnna, O. Pilla, M. Montagna, G. Ruocco, G. Signorelli, and V. Mazzacurati, Phys. Rev. B **52**, 3346 (1995); V. Martín-Mayor, G. Parisi, and P. Verrocchio, cond-mat/9911462, Phys. Rev. E (to be published).
[22] P. Turchi, F. Ducastelle, and G. Treglia, J. Phys. C **15**, 2891 (1982).
[23] See, e.g., G. Parisi, *Statistical Field Theory* (Addison-Wesley, New York, 1988).
[24] A. Georges, G. Kotliar, W. Kranth, and M. Rozenberg, Rev. Mod. Phys. **68**, 13 (1996).
[25] N. Furukawa, in *Physics of Manganites*, edited by T.A. Kaplan and S.D. Mahanti (Kluwer Academic/Plenum Publishers, New York, 1999).
[26] T. Hotta, Y. Takada, H. Koizumi, and E. Dagotto, Phys. Rev. Lett. **84**, 2477 (2000).
[27] D. Khomskii, cond-mat/0004034 (unpublished).
[28] M.R. Ibarra, P.A. Algarabel, C. Marquina, J. Blasco, and J. García, Phys. Rev. Lett. **75**, 3541 (1995).
[29] C.H. Booth, F. Bridges, G.H. Kwei, J.M. Lawrence, A.L. Cornelius, and J.J. Neumeier, Phys. Rev. Lett. **80**, 853 (1998).
[30] We remark that we have chosen these four families of fields for simplicity, but this is not a limitation of the method. More exotic ordering as canted or helicoidal can be also considered.
[31] See, e.g., T.S. Chihara, *An Introduction to Orthogonal Polynomials* (Gordon & Breach, New York, 1978).
[32] This strategy for minimizing errors has been pushed to its limits in H.G. Ballesteros, L.A. Fernández, V. Martín-Mayor, A. Muñoz Sudupe, G. Parisi, and J.J. Ruiz-Lorenzo, Phys. Lett. B **400**, 346 (1997); Nucl. Phys. B: Field Theory Stat. Syst. **512[FS]**, 681 (1998); Phys. Rev. B **58**, 2740 (1998).
[33] In fact, what one calculates is the 50th orthogonal polynomial (see Appendix), which requires 50 multiplications by the matrix $\mathcal{T}$, as the calculation that the 50th moment would have needed. Extracting the 50th orthogonal polynomial from the moments without use of the recursion relations, would have required the calculation of 99 moments. In the text, the word *moment* has been used in this somehow ambiguous way.
[34] M.J. Calderón, J.A. Vergés, and L. Brey, Phys. Rev. B **59**, 4170 (1999).
[35] This is a rather crucial step, because our estimation of both $\mathcal{F}_{\mathrm{Fer}}(\mathcal{M})$ and $\mathcal{F}_{\mathrm{Fer}}(0)$ is statistical: we average over the random vector v, see Eq. (31), and over the spin configurations. The point is that the *difference* of two quantities can have an enormously decreased statistical error if they are very correlated. Indeed, we have used the same random vectors for all the values of $\mathcal{M}$, and the same random-numbers sequence for the extraction of the spin configurations. We estimate that, in this way the variance on the difference decreases by a factor of ten, if compared with a single estimate of $\mathcal{F}_{\mathrm{Fer}}(\mathcal{M})$, and therefore a factor of 100 has been gained on computer time.
[36] H. Koizumi, T. Hotta, and Y. Takada, Phys. Rev. Lett. **81**, 3803 (1998).
[37] J. Fontcuberta, V. Laukhin, and X. Obradors, Phys. Rev. B **60**, 6266 (1999).
[38] J.M. de Teresa, C. Ritter, M.R. Ibarra, P.A. Algarabel, J.L. García-Muñoz, J. Blasco, J. García, and C. Marquina, Phys. Rev. B **56**, 3317 (1997).
[39] H.Y. Hwang, S.-W. Cheong, P.G. Radaelli, M. Mareizo, and B. Batlogg, Phys. Rev. Lett. **75**, 914 (1995).
[40] R.P. Borges, F. Ott, R.M. Thomas, V. Skumryev, J.M.D. Coey, J.I. Arnaudas, and L. Ranno, Phys. Rev. B **60**, 12 847 (1999).
[41] V.S. Amaral *et al.*, J. Magn. Magn. Mater. (to be published).